Research Article | Vol. 29, No. 18 / 30 Aug 2021 / Optics Express 28741
Optics EXPRESS

Frequency upconversion imaging based on Hadamard coding

YuQi Jiang,[1] WeiJi He,[1] TianYi Mao,[1,2] GuoHua Gu,[1,*] and Qian Chen[1]

[1]Jiangsu Key Laboratory of Spectral Imaging and Intelligence Sense, Nanjing University of Science and Technology, Nanjing 210094, China
[2]School of Geographic and Biologic Information, Nanjing University of Posts and Telecommunications, Nanjing 210023, China
*gghnjust@mail.njust.edu.cn

Abstract: A frequency upconversion imaging based on Hadamard coding is presented to remove the distorting effect on condition that the pump beam is tightly focused to optimize the conversion efficiency. The distortion caused by the convolution between the object field and the pump field is ascribed to the point spread function effect. In order to remove the blurring in an upconversion imaging system optimized by tight focused pump, the object is encoded by measurement matrices and the corresponding intensity of the converted field is measured. Thus the intensity distribution of the object can be calculated accurately by the measurements and the measurement matrix. The signal-to-noise ratio (SNR) is improved by employing the Hadamard matrix since the intensity of measured converted signal is far larger than the intensity of each pixel. The experimental results show the proposed method removes the distorting effect caused by the convolution. The converted image still has sharp edges on condition that the conversion efficiency is optimized by tight focusing the pump beam.

1. Introduction

The upconversion imaging technology is a promising alternative to the infrared imaging due to the low background noise level [1–4]. Normally, the upconveriosn imaging is based on quasi-phase match and the general formulation has been proposed in [5,6]. An important aspect of an upconversion system is the conversion efficiency. High conversion efficiency typically requires a sufficiently strong pump in a quadratic transparent crystal with a large optical nonlinearity [7–10]. The optimization of conversion efficiency by tight focusing the pump beam has been proposed and the method is applied in high sensitivity single-photon frequency upconversion detection [11–16]. Unfortunately, the optimization exists limitations in upconversion imaging systems. Although the frequency-converted field exhibits a similarity with the input field in the upconversion imaging setup, the converted field is distorted due to the spatial bandwidth of the phase-matching function and the limited spatial extent of the pump mode [17]. In the past, the distorting effect has been investigated [18]. Besides, a trade-off between the upconversion efficiency and the image quality caused by the convolution function of the input fields is revealed [5]. The convolution function is ascribed to a spatial filtering relating to the point spread function, which has been proved by several works [19–21]. Thus a large pump beam diameter in the nonlinear crystal contributes to removing the distorting effect but reduces the conversion efficiency.

The Digital Micro-mirror Device (DMD) is one of the most common opto-electro devices and consists of a micro-mirror array on a CMOS memory unit [22,23]. An advantage of the DMD is the incident beam is able to be modulated in spatial by DMD with high pattern refresh frequency. It is possible to measure the intensity of each pixel on the object field via using DMD modulate the input field in spatial. Theoretically, if the advantage of DMD and the upconversion imaging are combined, the distorting effect can be removed.

#425717 https://doi.org/10.1364/OE.425717
Journal © 2021 Received 23 Mar 2021; revised 14 Jul 2021; accepted 12 Aug 2021; published 23 Aug 2021

Optics EXPRESS

In this paper, an upconversion imaging of focused pump beam based on Hadamard coding is proposed. The distorting effect in upconversion imaging is removed by measuring the converted intensity of the encoded object field. Then the image can be reconstructed by the measurements and projected patterns. The simulation and the experimentally obtained reconstructed image are presented to show the effect of the proposed method. Besides, the influence of tightly focusing the pump beam to optimize the conversion efficiency on image quality is discussed by comparing the two groups of reconstructed images. This paper is organized with 5 sections. The formula model of the upconversion imaging is demonstrated in section 2. The simulation and the experimental result are presented in section 3. A comparison of the converted image with the tighter focused pump beam is investigated in section 4. The conclusion of proposed method and the discussion of the improvement are summarized in Section 5.

2. Theory

Signal upconversion treated in this paper is achieved via sum frequency generation (SFG). It is assumed that the amplitudes of the object field, pump field and upconverted field can be approximated as being constant throughout the entire interaction length of the nonlinear crystal. The pump is a monochromatic coherent field with a frequency ω_2 and focused by a lens with the focal length $f1$. The object field is a coherent state with a frequency ω_1. The SFG describes the energy transfer from the object field with frequency ω_1 by mixing with a pump field of frequency ω_2. The generated converted field frequency ω_3 equals the sum of the input and pump frequencies

$$\omega_3 = \omega_1 + \omega_2. \tag{1}$$

Figure 1 shows the model of an upconversion imaging system optimized by focusing the pump beam. The object field and the pump field located on the focal plane of $L1'$ are combined by a dichroic mirror. Then, the mixing field is focused into the nonlinear crystal by the achromatic lens $L1'$. It is assumed that both field is focused to the center of the crystal. The converted light is collimated by $L2'$.

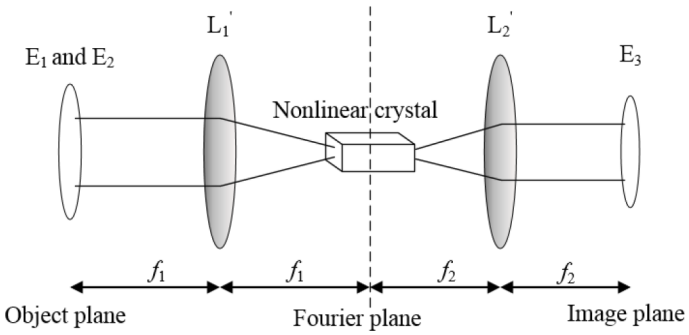

Fig. 1. The model of an upconversion imaging system; The object field E1 and the pump field E2 located on the focal plane of a $L1'$ are combined (not depicted in Fig. 1). Both fields are focused to the Fourier plane inside a nonlinear crystal. The generated upconverted field E3 is located on the image plane.

E_1 stands for the object field and E_2 stands for the pump field. Normally, E_2 has a Gaussian profile. The converted field $E_3(x, y)$ is the result of the upconversion process between E_1 and E_2 and (x, y) is the coordinate on image plane. According to [5], when considering the plane wave

Optics EXPRESS

approximation, the upconverted field is given by:

$$I_3(x,y) = \frac{8\pi d_{eff}^2 L^2 \lambda_1^2 f_1^2}{n_2 n_3 f_2^2 \lambda_3^4 \cos^2\theta w_0^2} P_{Gauss} \left| E_1(-\frac{\lambda_3 f_2}{\lambda_1 f_1}x, -\frac{\lambda_3 f_2}{\lambda_1 f_1}y) \otimes \left(\frac{\pi w_0^2}{(\lambda_3 f_2)^2} e^{-\frac{x^2+y^2}{\left(\frac{\lambda_3 f_2}{\pi w_0}\right)^2}} \right) \right|^2 \tag{2}$$

where d_{eff} is the effective second order nonlinearity of the nonlinear crystal. L is the length of nonlinear crystal. $f_i (i = 1, 2)$ are the focal length of L1′ and L2′ separately. λ_1 is the wavelength of the light emitted from the object and λ_2 is the wavelength of the pump beam. The upconverted wavelength λ_3 is determined by the energy conservation law: $\frac{1}{\lambda_3} = \frac{1}{\lambda_1} + \frac{1}{\lambda_2}$. θ is the variation of the angle for the signal light considering the effective interaction length. w_0 is the pump beam radius on the Fourier plane of L1′. Eq. (2) is also discussed in [24]. Figure 1 shows w_0 depends on the focal length of L1′ and the radius of Gaussian profile. Eq. (2) indicates if w_0 is large enough to transforming the normalized convolution function into a delta-function, a perfect upconverted replica of the original image. However, the upconversion efficiency benefits from a small w_0, which means the image is distorted due to the convolution function. Hence, a tightly focused pump beam results the converted image has no sharp edge.

Here, a binary DMD and a photomultiplier tube (PMT) are employed to remove the distorting effect. The object field is encoded by a binary DMD with Hadamard matrices. The converted intensity profile $I_3(x, y)$ is collected by a lens and measured by a single-pixel detector such as the PMT. Thus $E_i(x, y)$ $(i = 1, 2, 3)$ and $I_i(x, y)$ $(i = 1, 2, 3)$ are discretized to matrices $E_{im}(x, y)$ $(i = 1, 2, 3)$ and $I_{im}(x, y)$ $(i = 1, 2, 3)$ in the following. According to Eq. (2), the measured intensity of the upconverted field corresponding to $I_{1m}(x_0, y_0)$ is defined as

$$I_{3s}(x,y) = \sum I_{3m}(x,y) \tag{3}$$

where the symbol $\sum$ means summing the whole upconverted intensity field. Therefore, the upconverted intensity corresponding to the position $(-\frac{\lambda_3 f_2}{\lambda_1 f_1}x_0, -\frac{\lambda_3 f_2}{\lambda_1 f_1}y_0)$ takes the form

$$\begin{aligned} I_{3s}(x_0,y_0) &= \sum I_{3m}(x,y) \\ &= \sum \frac{8\pi d_{eff}^2 L^2 \lambda_1^2 f_1^2}{n_2 n_3 f_2^2 \lambda_3^4 \cos^2\theta w_0^2} P_{Gauss} \left| E_{1mxy}(-\frac{\lambda_3 f_2}{\lambda_1 f_1}x, -\frac{\lambda_3 f_2}{\lambda_1 f_1}y) \otimes E_P \right|^2 \end{aligned} \tag{4}$$

where E_P stands for the Gauss distribution of the pump field. E_{1xy} is given by

$$E_{1mxy}(-\frac{\lambda_3 f_2}{\lambda_1 f_1}x, -\frac{\lambda_3 f_2}{\lambda_1 f_1}y) = \begin{cases} E_{1m}(-\frac{\lambda_3 f_2}{\lambda_1 f_1}x, -\frac{\lambda_3 f_2}{\lambda_1 f_1}y), & -\frac{\lambda_3 f_2}{\lambda_1 f_1}x = x_0, -\frac{\lambda_3 f_2}{\lambda_1 f_1}y = y_0 \\ 0, & \text{else} \end{cases} \tag{5}$$

Hence, $I_{3s}(x_0, y_0)$ stands for the upconverted intensity of the corresponding position on the object plane. The upconverted efficiency is defined as the ratio of the power at the generated output frequency ω_3 and the input frequency ω_1. Here, the upconverted efficiency of the position (x_0, y_0) is expressed by the ratio of the intensity at ω_3 and ω_1, which is represented as:

$$\eta(x_0,y_0) = \sum \frac{8\pi d_{eff}^2 L^2 \lambda_1^2 f_1^2}{n_2 n_3 f_2^2 \lambda_3^4 \cos^2\theta w_0^2} P_{Gauss} \left| E_{1mxy0}(-\frac{\lambda_3 f_2}{\lambda_1 f_1}x, -\frac{\lambda_3 f_2}{\lambda_1 f_1}y) \otimes E_P \right|^2 \tag{6}$$

where E_{1xy0} is given by

$$E_{1mxy0}(-\frac{\lambda_3 f_2}{\lambda_1 f_1}x, -\frac{\lambda_3 f_2}{\lambda_1 f_1}y) = \begin{cases} 1, & -\frac{\lambda_3 f_2}{\lambda_1 f_1}x = x_0, -\frac{\lambda_3 f_2}{\lambda_1 f_1}x = y_0 \\ 0, & \text{else} \end{cases} \tag{7}$$

Optics EXPRESS

For the intensity matrix I_1 including $N \times N$ elements, the measurement corresponding to the projected matrix $H_n(n = 1, 2, \ldots, N^2)$ can be expressed as

$$M_n = H_{nv} I_{1v} \cdot \eta_v, \tag{8}$$

where H_{nv} is a $1 \times N^2$ vector resized by the projected matrix H_n, which indicates the DMD status ('1' or '0') of the corresponding pixel. I_{1v} is a $N^2 \times 1$ vector resized by I_{1m}, which stands for the intensity of the object. η_v is a $N^2 \times 1$ vector resized by η. The symbol $\cdot$ means the dot production. The coding matrix H is expressed as a concatenation of these projected matrices, which is formulated as

$$H = [H_1 \; H_2 \; \cdots \; H_{N^2}]. \tag{9}$$

where H has $N^2 \times N^2$ elements. The $N^2 \times 1$ measurements vector M is written as

$$M = H I_{1v} \cdot \eta_v, \tag{10}$$

According to Eq. (6) and Eq. (7), each element of $\eta(x_0, y_0)$ is positive number. Thus the $N^2 \times 1$ vector η_{vi} is defined as

$$\eta_{vi}(n) = \frac{1}{\eta_v(n)}. \tag{11}$$

Considering the transposed Hardmard matrix is itself and η_{vi} is a vector that each element is positive number, the object is reconstructed by

$$I_{1v} = H_t M \cdot \eta_{vi}. \tag{12}$$

where H_t the transposed matrix of H.

3. Result

3.1. Setup

The layout of the experiment is described in Fig. 2. A pulse fiber laser at 1550 nm with 200 mW peak power is the signal beam source. The pulse duration is 10 ns and the repetition rate is 10 kHz. A polarization maintained fiber transfers the 1550 nm pulse to the fiber collimator C1. The half wave plate HWP1 is used to set the the polarization state of the collimated 1550 nm pulse. The 1550 nm pulse propagates through a test pattern and the 4f system, which consists of lenses L1 (f_1 = 75 mm) and L2 (f_2 = 75 mm). Then the 1550 nm pulse is modulated by a binary DMD. The DMD consists of 1024 × 768 digital micro-mirrors of size 13.68 μm × 13.68 μm. Each mirror is independently controlled and can steer light in two digital positions (12° and −12°). A region with 512 × 512 pixels is employed to modulate the object. The DMD rotating with 45° as shown in Fig. 2 to ensure that the reflected 1550 nm pulse can be focused into the PPLN. The modulated 1550 nm pulse is reflected to the 4f system consisting of L3 (f_3 = 75 mm) and L4 (f_4 = 75 mm) by changing the state of the corresponding micromirrors of the DMD. The measured peak power of the reflected 1550 nm pulse is 40 mW due to the DMD window option wavelength and the lenses.

The pump beam source is a continuous wave fiber laser at 1950 nm with 400 mW power. A polarization maintained fiber transfers the 1950 nm beam to the fiber collimator C2. The polarization state of the collimated pump beam is set by the half wave plate HWP2. The modulated 1550 nm pulse and the pump beam are combined by a dichroic mirror (DM). The mixing laser is focused into a PPLN crystal by the achromatic lens L5 (f_5 = 100 nm). The PPLN is antireflection (AR)-coated for high transmission at 1550 nm and 1950 nm on the side near L5 to reduce the loss of power. The opposite side is antireflection (AR)-coated for high transmission at 863 nm. The PPLN is 20 mm long and 2 mm width of a poled channel with a thickness of 1

Optics EXPRESS

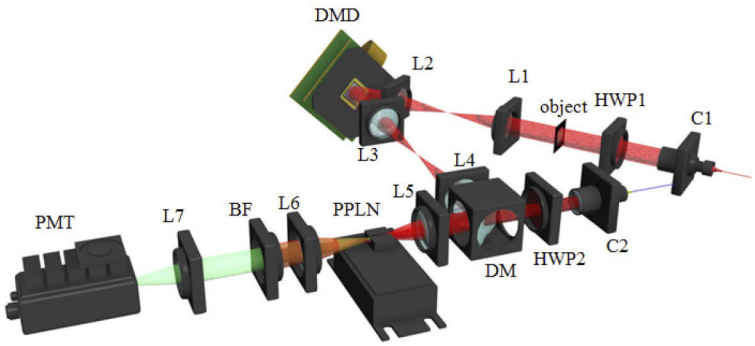

Fig. 2. The setup of the experiment. C1and C2 are the fiber collimator connected on the signal beam source and pump beam source separately. HW1 and HW2 are half wave plates. L1, L2, L3, L4, L6 and L7 are lenses. L5 is a achromatic lens. DM is a dichroic mirror. BF is a band-pass filter.

mm. The poling period of PPLN is 24.1 ± 0.1 μm. A temperature-controlled mount ensures millikelvin stability of the crystal at 58.4 ± 0.1 $^{\circ}C$. The frequency converter is based on collinear type-0 quasi-phase matching shown as follows:

$$1950\,\text{nm (e)} + 1550\,\text{nm (e)} \rightarrow 863\,\text{nm (e)}. \tag{13}$$

The upconverted signal propagates through lens L6 (f_6 = 100 mm) and lens L7 (f_7 = 50 mm) . A band-pass filter is placed between L6 and L7 to select the wavelength. The central wavelength of the band-pass filter is 860 nm and the full width at half maximum (FWHM) is 10 nm. The transmittance of the band-pass filter at 860 nm is about 40%. The collected converted light is measured by a PMT, which is sensitive along a wide spectral range from 300 nm to 890 nm. Considering the loss of power when the object field propagates the lenses and is modulated by DMD, the minimum peak power that can be detected by our system is 5 mW.

3.2. Simulation and experiment

In this subsection, the simulation of the direct image at converted wavelength and the reconstructed converted image are demonstrated. Then, experimentally obtained and theoretically calculated results are compared.

Figure 3(a) shows the process of our method. In Fig. 3(a), the pattern is organized by element '1' (white) or '0' (black). Figure 3(b) shows the theoretically calculated upconverted image on condition that the camera is mounted on the image plane of L6. In order to compare the object and the converted image, the direct image is acquired by an camera (Bobcat-320 Cooled smart InGaAs camera, manufactured by Xenics) at 1550 nm and resized to 64 × 64 pixels. I_1 is the intensity profile of the object and I_2 is the intensity profile of the pump beam. I_3 stands for the distribution of the converted intensity field on the focal plane of L6. $E_i(i = 1, 2, 3)$ is the amplitude corresponding to $I_i(i = 1, 2, 3)$. I_3 shows that the point spread function effect contributes to the object edge strongly blurring in an upconversion system optimized by focusing the pump beam. The distorting is caused by the convolution of the object field E1 and the focused Gauss field.

Then, the theoretically calculated converted image reconstructed by the proposed method is shown in Fig. 3(c). Here, it is assumed that the focused object field is overlapped by the focused pump beam in the PPLN, otherwise the object field cannot be converted completely. M is a single column vector and each element stands for the measured converted intensity of corresponding pattern. The measurement matrix H_t is the inverse of the Hadamard matrix with 4096 × 4096

Optics EXPRESS

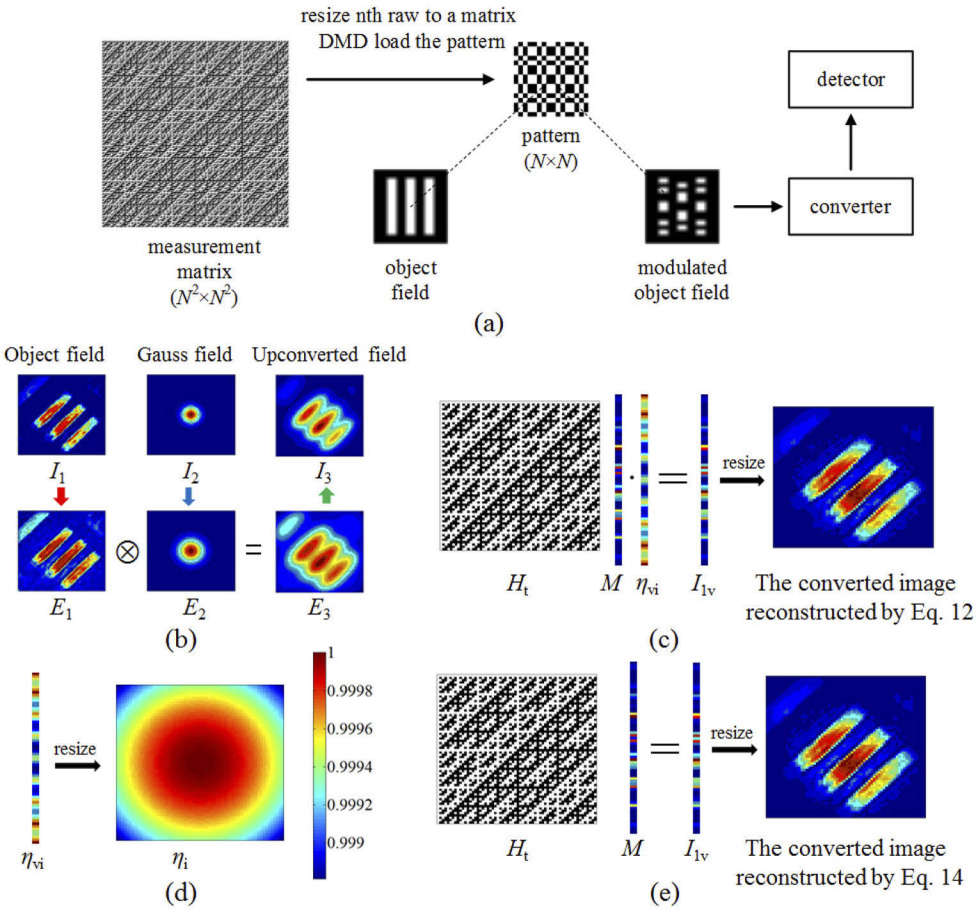

Fig. 3. (a) The process of our method. (b) The theoretically calculated direct image at converted wavelength. (c) The theoretically calculated upconverted image reconstructed by proposed method. (d) The matrix η_i resized by η_{vi} and its color bar. (e) The simulation of reconstructing the converted image by simplified method.

elements. η_{vi} is a single column vector with 4096 elements and each element stands for the multiplicative inverse of the upconversion efficiency of corresponding pixel. The single column vector I_{1v} is calculated by M, H_t and η_{vi} according to Eq. (12). Thus the converted image is created by resizing I_{1v} to a matrix with 64×64 pixels. Figure 3(c) shows the distorting of the image is removed and the edge of converted object is still sharp. In particular, η_v is a normalized 64×64 matrix resized by η_{vi} and its distribution is shown in Fig. 3(d). In Fig. 3(d), the color bar shows the maximum value of η_v is approximately to the minimum value of η_v. Hence, our method can be simplified and Eq. (12) is rewritten to

$$I_{1v} = H_t M. \tag{14}$$

The simulation result of Eq. (14) is shown in Fig. 3(e). Comparing Fig. 3(c) and Fig. 3(e), the reconstructed image is not distorted, which also indicates the conversion efficiency within the Field of View (FOV) is approximated to a constant approximately and the contribution of η_{vi} in Eq. (12) can be neglected. The comparison of the simulation and the experimental result is shown in Fig. 4.

Optics EXPRESS

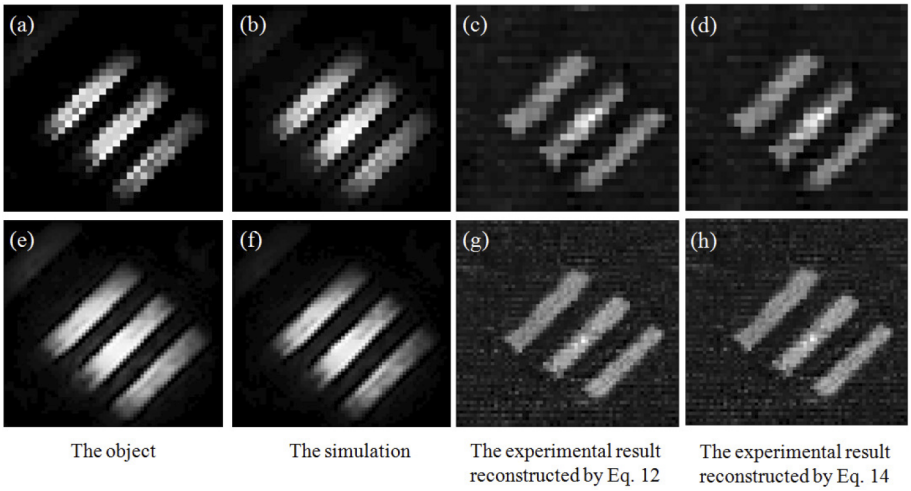

Fig. 4. (a) Direct image of the object illuminated by 1550 nm pulse. The image is resized to 32×32 pixels. (b) The simulation of reconstructing the converted image including 32×32 pixels by proposed method. (c) The converted image including 32×32 pixels reconstructed by Eq. (12). (d) The converted image including 32×32 pixels reconstructed by Eq. (14). (e) Direct image of the object illuminated by 1550 nm pulse. The image is resized to 64×64 pixels. (f) The simulation of reconstructing the converted image including 64×64 pixels by proposed method. (g) The converted image including 64×64 pixels reconstructed by Eq. (12). (h) The converted image including 64×64 pixels reconstructed by Eq. (14).

Figure 4 shows reconstructed converted image in different scale. Figure 4(a) and Fig. 4(e) are the direct image of the object. Figure 4(b) and Fig. 4(f) are the simulation results. Comparing the direct images at 1550 nm with the corresponding simulation results, the reconstructed image is a replica of the direct image on condition that the normalized convolution function cannot be transformed into a delta-function. Besides, Fig. 4(c) and Fig. 4(g) show the intensity profile of experimental obtained image reconstructed by Eq. (12) is similar to the object, which are also agreement with the simulation in Fig. 4(b) and Fig. 4(f) separately. The resolution of Fig. 4(c) and Fig. 4(g) are 219.2 μm and 109.6 μm. Comparing the measured and calculated intensity profiles, note that the object edges is still clearly seen in Fig. 4(c) and Fig. 4(f). The intensity profile of the converted object in higher resolution is not blurring and the effect of the point spread function smearing out the edges of the image is removed. Figure 4(d) and Fig. 4(h) shows the converted image reconstructed by Eq. (14). Comparing them with the images reconstructed by Eq. (12), that η_v is approximated to a constant has few influence on the reconstructed image.

However, Fig. 4(c) and Fig. 4(g) are hampered by the noise comparing with the simulation. The reasons are listed as follows. Firstly, the simulation result does not consist the noise but the noise from the detector exists in experiment. Although Fig. 4(d) and Fig. 4(h) show that the the influence of the conversion efficiency on the intensity profile can be neglected, low conversion efficiency leads to the SNR of measurements reduced. Secondly, the DMD window option wavelength reduces the intensity of the object and the converted power is limited. Thirdly, although the signal beam and the pump beam are focused with a achromatic lens, the conversion efficiency and the matrix η' in Eq. (7) depends on the spatial overlap in the focus plane of the two interacting beams. The center of two beams are overlapped perfectly in simulation while the overlapping is imperfect in experiment. Optimizing the upconversion efficiency and reducing the loss of propagation can improve the reconstructed image.

Optics EXPRESS

4. Analysis

In this section, the quality of reconstructed image with a tighter focused pump beam is discussed. In order to show the advantage of presented method, the pump beam is focused by two achromatic lenses separately and the reconstructed images are compared. The pump beam is focused by an achromatic lens (f = 100 mm) and the setup is shown in Fig. 3. Then, the output is enhanced by using another achromatic lens (f = 60 mm) to tighter focusing the pump beam. The experimentally obtained is shown in Fig. 5.

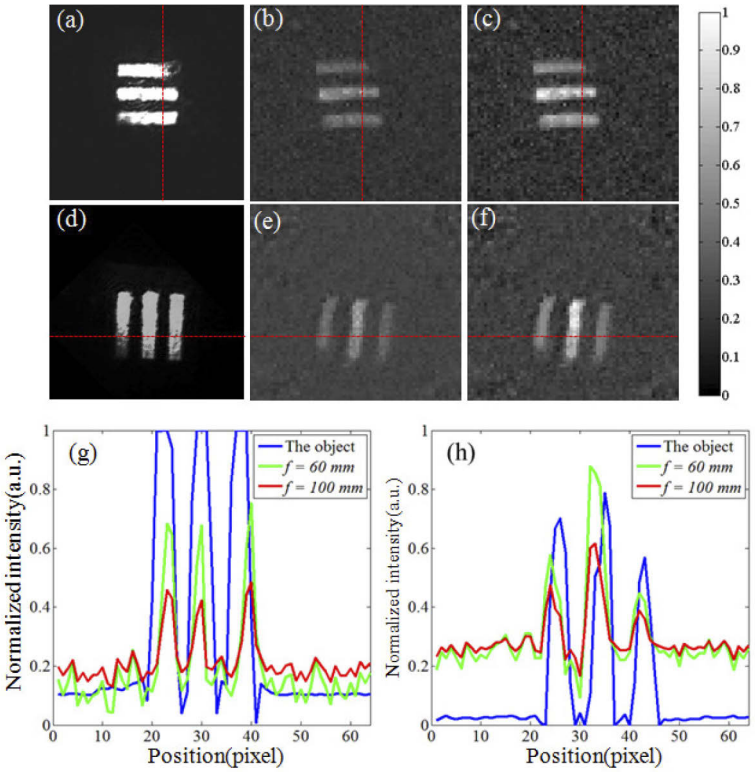

Fig. 5. (a) Direct image at 1550 nm. (b) The reconstructed image of (a). The pump beam is focused by an achromatic lens (f = 100 mm) (c) The reconstructed image of (a). The pump beam is focused by an achromatic lens (f = 60 mm) (d) Direct image of at 1550 nm. (e) The reconstructed image of (d). The pump beam is focused by an achromatic lens (f = 100 mm) (f) The reconstructed image of (d). The pump beam is focused by an achromatic lens (f = 60 mm) (g) The normalized pixel-value along the red dashed line in (a), (b) and (c). (h) The normalized pixel-value along the red dashed line in (d), (e) and (f).

Figure 5(a) and Fig. 5(d) are the direct images of the object illuminated by the 1550 nm pulse. Figure 5(b) and Fig. 5(e) are the reconstructed images of the pump beam focused by the first achromatic lens (f = 100 mm). Then, the setup is optimized by using another achromatic lens (f = 60 mm) to focus the pump beam and achieves higher conversion efficiency. The optimized reconstructed images are shown in Fig. 5(c) and Fig. 5(f). Figure 5(c) and Fig. 5(f) shows that the reconstructed image alone vertical and horizontal still has sharp edges. The image is not blurring with the pump beam size decreasing on the Fourier plane. The results indicate that the conversion efficiency of high-frequency components is approximately to the low-frequency components. The distorting effect caused by the convolution in Eq. (2) is removed in our method.

Optics EXPRESS

Beside, Fig. 5(g) and Fig. 5(h) shows the presented method takes advantage of the tight focused pump beam. The normalized intensity curve shows the contribution of tighter focused pump beam to the conversion efficiency. The blue curve in Fig. 5(g) and Fig. 5(h) are the normalized intensity of the resized object in Fig. 5(a) and in Fig. 5(d) separately. The red curve and green curve in Fig. 5(g) stand for the normalized intensity of Fig. 5(b) and Fig. 5(c). The red curve and green curve in Fig. 5(h) stand for the normalized intensity of Fig. 5(e) and Fig. 5(f). Figure 5(g) shows the tighter focused pump beam enhances the intensity of converted light. Note that the normalized intensity of the background noise is about 0.2 and the SNR is improved by tighter focusing the pump beam. Moreover, the peak signal noise ratio (PNSR) of Fig. 5(b) is 12.30 dB while the PNSR of Fig. 5(c) is 16.54 dB. The comparison indicates the noise is reduced due to the optimized conversion efficiency. In Fig. 5(d), the power of 1550 nm pulse illuminating the object is reduced and the measured peak power of the reflected 1550 nm pulse is 20 mW. Figure 5(h) shows the low converted intensity reduces the SNR. The PNSR of Fig. 5(e) is 13.44 dB while the PNSR of Fig. 5(f) is 11.84 dB. According to PNSR of Fig. 5(b), Fig. 5(c), Fig. 5(e) and Fig. 5(f), the SNR of reconstructed image can benefit from the tighter focusing pump beam.

5. Conclusion

In conclusion, a frequency upconversion imaging method based on Hadamard coding is demonstrated to remove the distorting caused by the convolution. The proposed method consists of two steps: 1) The converted intensity of the encoded object measured by a single-pixel detector accurately. 2) The object is reconstructed by the measurements and measurement matrices. Experimental results show the reconstructed image has sharp edges although the pump beam radius at the center of the PPLN is not sufficiently large. The spatial resolution does not reduce with a tighter focused pump beam. Further, the conversion efficiency and the SNR are benefited from the tighter focused pump beam. The resolution of our method is mainly decided by the size of each mirror on the DMD and the sensitivity of the system. On the one hand, the pixel size of reconstructed image increases linearly with the size of each mirror on DMD increasing. On the other hand, the small size of mirror on DMD means that the converted signal is weak, which requires high sensitive and high conversion efficiency. Thus a high conversion efficiency converter and a DMD with small size mirror contributes to the resolution. It is noted that the pixel number of the reconstructed image is limited by the hardware. As is known to us, the image created by the computation imaging technology is not beyond 256×256 pixels, which indicates there is a possibility that our method can reach this resolution. Beside, using the presented method to realize high-definition imaging with more pixels can benefit from the development of the hardware.

Although frequency upconversion imaging method based on Hadamard coding is applied on near-infrared imaging, the proposed method can be extend to mid-infrared (MIR) wavelengths. According to the principle of frequency, if the presented method is extended to MIR, the nonlinear crystal and the pump beam should be designed. Fortunately, the frequency upconversion at MIR has been investigated, which means that the proposed method is able to applied on mid-infrared (MIR) wavelengths.

Funding. Fundamental Research Funds for the Central Universities (30919012103); National Natural Science Foundation of China (61875088, 62005128).

Disclosures. The authors declare that there are no conflicts of interest related to this article

Data availability. No data were generated or analyzed in the presented research.

References

1. P. S. Kuo, J. S. Pelc, O. Slattery, Y. Kim, M. M. Fejer, and X. Tang, "Reducing noise in single-photon-level frequency conversion," Opt. Lett. **38**(8), 1310 (2013).
2. P. S. Kuo, J. S. Pelc, C. Langrock, and M. M. Fejer, "Using temperature to reduce noise in quantum frequency conversion," Opt. Lett. **43**(9), 2034 (2018).

Optics EXPRESS

3. J. S. Dam, P. Tidemand-Lichtenberg, and C. Pedersen, "Room-temperature mid-infrared single-photon spectral imaging," Nat. Photonics **6**(11), 788–793 (2012).
4. A. Barh, C. Pedersen, and P. Tidemand-Lichtenberg, "Ultra-broadband mid-wave-ir upconversion detection," Opt. Lett. **42**(8), 1504–1507 (2017).
5. C. Pedersen, E. Karamehmedović, J. S. Dam, and P. Tidemand-Lichtenberg, "Enhanced 2d-image upconversion using solid-state lasers," Opt. Express **17**(23), 20885–20890 (2009).
6. J. S. Dam, C. Pedersen, and P. Tidemand-Lichtenberg, "Theory for upconversion of incoherent images," Opt. Express **20**(2), 1475–1482 (2012).
7. K. Huang, X. Gu, H. Pan, E. Wu, and H. Zeng, "Synchronized fiber lasers for efficient coincidence single-photon frequency upconversion," IEEE J. Sel. Top. Quantum Electron. **18**(2), 562–566 (2012).
8. A. K. Hansen, P. E. Andersen, O. B. Jensen, B. Sumpf, G. Erbert, and P. M. Petersen, "Highly efficient single-pass sum frequency generation by cascaded nonlinear crystals," Opt. Lett. **40**(23), 5526–5529 (2015).
9. H. Pan, H. Dong, H. Zeng, and W. Lu, "Efficient single-photon counting at 1.55 μ m by intracavity frequency upconversion in a unidirectional ring laser," Appl. Phys. Lett. **89**(19), 191108 (2006).
10. M. A. Albota and F. N. Wong, "Efficient single-photon counting at 1.55 μm via frequency upconversion, in Postdeadline Papers Book," *Conf. on Lasers and Electro-Optics/Quantum Electronics & Laser Science Conference (CLEO/QELS)*, (2003).
11. G. Boyd and D. Kleinman, "Parametric interaction of focused gaussian light beams," J. Appl. Phys. **39**(8), 3597–3639 (1968).
12. R. L. Sutherland, *Handbook of nonlinear optics* (CRC press, 2003).
13. D. A. Kleinman, A. Ashkin, and G. Boyd, "Second-harmonic generation of light by focused laser beams," Phys. Rev. **145**(1), 338–379 (1966).
14. R. W. Boyd, *Nonlinear optics* (Elsevier, 2003).
15. X. Gu, K. Huang, H. Pan, E. Wu, and H. Zeng, "Efficient mid-infrared single-photon frequency upconversion detection with ultra-low background counts," Laser Phys. Lett. **10**(5), 055401 (2013).
16. Q. Zhou, K. Huang, H. Pan, E. Wu, and H. Zeng, "Ultrasensitive mid-infrared up-conversion imaging at few-photon level," Appl. Phys. Lett. **102**(24), 241110 (2013).
17. F. Steinlechner, N. Hermosa, V. Pruneri, and J. P. Torres, "Frequency conversion of structured light," Sci. Rep. **6**(1), 21390 (2016).
18. J. Torres, A. Alexandrescu, and L. Torner, "Quantum spiral bandwidth of entangled two-photon states," Phys. Rev. A **68**(5), 050301 (2003).
19. R. Tang, W. Wu, X. Li, H. Pan, E. Wu, and H. Zeng, "Two-dimensional infrared and mid-infrared imaging by single-photon frequency upconversion," J. Mod. Opt. **62**(14), 1126–1131 (2015).
20. K. Huang, X. Gu, H. Pan, E. Wu, and H. Zeng, "Few-photon-level two-dimensional infrared imaging by coincidence frequency upconversion," Appl. Phys. Lett. **100**(15), 151102 (2012).
21. H. Maestre, A. J. Torregrosa, and J. Capmany, "Ir image upconversion using band-limited ase illumination fiber sources," Opt. Express **24**(8), 8581–8593 (2016).
22. M. Li, Y. Li, W. Liu, A. Lal, S. Jiang, D. Jin, H. Yang, S. Wang, K. Zhanghao, and P. Xi, "Structured illumination microscopy using digital micro-mirror device and coherent light source," Appl. Phys. Lett. **116**(23), 233702 (2020).
23. D. Dudley, W. M. Duncan, and J. Slaughter, "Emerging digital micromirror device (dmd) applications," in *MOEMS display and imaging systems*, vol. 4985 (International Society for Optics and Photonics, 2003), pp. 14–25.
24. A. Barh, P. J. Rodrigo, L. Meng, C. Pedersen, and P. Tidemand-Lichtenberg, "Parametric upconversion imaging and its applications," Adv. Opt. Photonics **11**(4), 952–1019 (2019).